RSC Mechanochemistry

Accepted Manuscript

This article can be cited before page numbers have been issued, to do this please use: G. Demily, N. KANIA, A. Ponchel and S. MENUEL, *RSC Mechanochem.*, 2026, DOI: 10.1039/D6MR00034G.

ROYAL SOCIETY OF CHEMISTRY

When breaking heterojunctions unlocks a reactive compromise in photomechanocatalytic phenol degradation over P25-TiO_2

Received 00th January 20xx,
Accepted 00th January 20xx

DOI: 10.1039/x0xx00000x

Guillaume Demily[a], Nicolas Kania[a], Anne Ponchel[a] and Stéphane Menuel[a] *

Mechanical activation and photochemical excitation are investigated for the environmental remediation of phenol using P25 TiO_2. Operating under a controlled low liquid-assisted grinding (LAG) regime with sequential H_2O_2 addition, this study demonstrates that mechanical energy effectively drives oxidative degradation in the absence of light. Multiscale characterization reveals that while the bulk crystalline integrity of the anatase and rutile phases is preserved, vibratory milling induces significant structural modifications and optical band gap narrowing. The physical disruption of anatase-rutile heterojunctions generates a defective surface layer that enables dark reactivity, which is further enhanced by simultaneous UV irradiation as the material remains distinctly photoactive. Operating in this state of reactive compromise, the system couples mechanical defect generation with the conservation of photocatalytic efficiency. Finally, green chemistry metrics highlight the significant environmental benefits of this nearly solvent-free photomechanocatalytic approach.

Introduction

The contamination of ecosystems by organic pollutants constitutes a critical environmental challenge, necessitating robust remediation technologies. Heterogeneous photocatalysis utilising titanium dioxide (TiO_2) remains one of the most extensively investigated Advanced Oxidation Processes (AOPs) for the mineralisation of these contaminants. Despite its maturity, this technology is intrinsically hindered by the rapid recombination of charge carriers and the difficulty of treating turbid or opaque media, thereby hampering its large-scale applicability.[1,2]

To circumvent these limitations, alternative approaches have been explored to enable catalyst activation through non-photonic energy sources. In this context, the exploitation of mechanical energy to initiate catalytic reactions in the liquid phase has gained significant traction. In such systems, where the catalyst is dispersed within a large solvent volume, activation is primarily derived from hydrodynamic phenomena (magnetic stirring, high-energy mixing) or acoustic events (sonochemistry). These stimuli activate tribocatalytic (solid-liquid/solid-solid friction)[3] or piezocatalytic (strain-induced deformation) mechanisms, enabling pollutant degradation or CO_2 reduction in the absence of light.[4,5] This approach exploits the polarization induced by a strain gradient, typically generated by sonoactivation[6] or high-energy agitation of materials in liquid suspension.[7] In this context, it has also been observed that mechanically activating rutile through high-energy milling in colloidal suspensions facilitates the degradation of organic pollutants.[8]

Nevertheless, it is crucial to distinguish these solution-based approaches from mechanochemistry in the strict sense.[9] The latter entails high-energy conditions, generally in the absence of solvent or in the presence of trace amounts of liquid[10] (Liquid-Assisted Grinding or LAG). In this regime, shear and impact forces are substantially higher surface reactivity. Mechanocatalysis has thus proven its capacity to perform complex organic syntheses, such as hydroformylation under a controlled atmosphere,[11] demonstrating that mechanical energy alone can surmount high activation barriers inaccessible via simple agitation.

Recently, several research groups have paved the way for the emergence of photomechanochemistry, which couples light irradiation with this high-energy mechanical activation. This domain has been primarily investigated within the fields of organic synthesis and materials science. Seminal works have demonstrated that this coupling facilitates the borylation of aryldiazonium salts,[12] the controlled oxidation of diphenylacetylene,[13] the synthesis of nanographenes,[14] and dehalogenation via photoreduction.[15] These studies suggest a unique synergy wherein mechanical input amplifies photochemical reactivity. Early efforts laid the groundwork by demonstrating the feasibility of related solvent-free photocatalysis.[16] Since then, the use of ball-milling to drive light-mediated reactions has been extensively reviewed[17] and successfully applied to complex systems, including solvent-minimized metallaphotoredox catalysis[18] and a broad range of general organic syntheses.[19] Additionally, the scope of photomechanochemistry has broadened to include resonant acoustic mixing, providing an efficient, media-free alternative for solid-state photochemistry[20] and scalable photoredox applications.[21]

In this study, we propose to extend the concept of photomechanochemistry to the field of environmental remediation. We introduce an approach coupling mechanocatalysis and photocatalysis, utilising the degradation of TiO_2-catalysed phenol as a robust model reference reaction. The oxidative degradation of phenol typically proceeds via the formation of hydroxylated aromatic intermediates, such as catechol, hydroquinone and benzoquinone, prior to undergoing ring cleavage into aliphatic compounds and ultimate mineralisation into CO_2 and H_2O (Scheme 1).[22] By monitoring this model reaction, we demonstrate that the combination of

[a] Univ. Artois, CNRS, Centrale Lille, Univ. Lille, UMR 8181, Unité de Catalyse et Chimie du Solide (UCCS), Rue Jean Souvraz, SP 18, 62300 Lens, France. E-mail: stephane.menuel@univ-artois.fr

† Supplementary Information available. See DOI: 10.1039/x0xx00000x

View Article Online DOI: 10.1039/D6MR00074C

mechanical activation and UV irradiation constitutes an effective approach for remediation requiring minimal water usage.

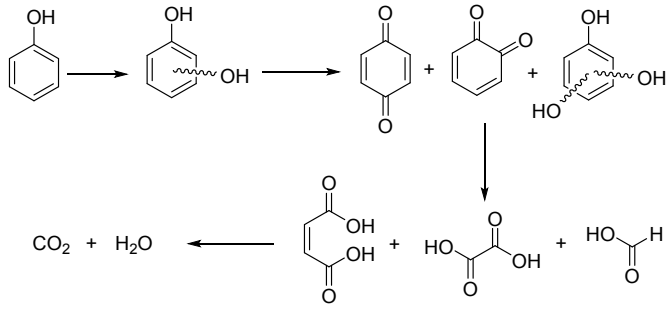

Scheme 1: Simplified oxidative degradation pathway of phenol.

Results and discussion

Comparative kinetic study between solution-based photocatalysis, mechanocatalysis and photo-mechanocatalysis

To establish a comparative reference in solution against the mechanochemical activation, the catalytic performance was first evaluated in a classical aqueous suspension. For this purpose, we employed P25-TiO_2[23], a benchmark commercial TiO_2 consisting of an 80:20 anatase-to-rutile phase mixture. Experiments were conducted in 10 mL of D_2O containing 5 mg of P25 and 0.1 mg of phenol, strictly defining a catalyst-to-pollutant mass ratio of R=50. As anticipated, the P25 catalyst remains inactive in the dark (Table 1, entry 1), whereas it efficiently degrades phenol under UV irradiation, exhibiting a pseudo-first-order rate constant of $k=30.09\times10^{-3}$ min^{-1} (Table 1, entry 2 and ESI)

The mechanochemical investigations were performed using a vibratory mill operating at 20 Hz. This specific frequency was established as the optimal operational limit following preliminary macroscopic observations with increasing the frequency to 25 Hz induced a rapid and severe compaction of the reaction medium within the first few minutes, effectively halting the necessary internal mixing dynamics. The reaction vessels were 50 mL zirconia jars loaded with 11 borosilicate glass beads (Ø 10 mm, average mass of 1.36 g) as grinding media. The selection of borosilicate glass for the beads is a deliberate safety choice. Matching the mechanical resistance and density of the grinding media to that of the custom borosilicate glass lid strictly mitigates the risk of shattering the transparent window upon impact. To enable *in situ* UV irradiation, the jars were equipped with a custom borosilicate glass lid, specifically selected for its high physical and chemical resistance to the extreme milling conditions. The wavelength-dependent optical transmission profile of this lid, confirming its transparency in the UV range, is provided in the Supplementary Information (ESI), alongside the specific reactor configuration.

To ensure a rigorous comparison with the solution-phase kinetics, the solid loading was scaled up to 4000 mg of P25 and 80 mg of phenol, thereby preserving the identical mass ratio R=50 across both scales. Transitioning to solvent-free mechanochemical conditions induces a radical shift in reactivity. To strictly isolate the role of the oxidant from rheological effects, two distinct control environments were investigated. First, under strictly anhydrous conditions involving dry milling (Table 1 entry 3 and entry 4), no significant phenol degradation was observed, regardless of whether mechanical activation is applied independently or coupled with UV irradiation.

This inhibition underscores that the catalyst cannot drive an oxidative cycle in the absence of a proton or oxygen source. Second, a "water-only" control was performed to assess the intrinsic capacity of Liquid-Assisted Grinding (LAG) to generate reactive species. Rather than a single initial liquid injection, which could drastically alter the powder bed rheology, water was added sequentially every 15 minutes. This "fed-batch" strategy ensured that the liquid-to-solid ratio (η) remained stable within a narrow range ($0.02\leq\eta\leq0.16$ $\mu L.mg^{-1}$) throughout the 120-minute reaction, strictly maintaining a low-LAG environment. This stability minimizes rheological fluctuations, thereby preventing potential shifts in energy transfer mechanisms. Despite this controlled liquid assistance, the activity remains marginal: $k=1.88\times10^{-3}$ min^{-1} under photo-mechanochemical coupling (Table 1, entry 6), and no significant degradation without UV (Table 1, entry 5). This lower activity compared to the classical aqueous suspension indicates that the in-situ generation of oxidizing species from these restricted amounts of water remains the primary kinetic bottleneck (Fig.1).

In aqueous suspension, water exists in very large excess, providing a reservoir for the production of reactive species. Conversely, under LAG (Liquid-Assisted Grinding)[24] conditions, the limited absolute water content inevitably constrains the overall production rate of H_2O_2 and radical species (typically evaluated as a mass-normalized flux in $mmol\cdot g^{-1}.h^{-1}$ in classical systems).[25] Consequently, the total oxidant flux remains insufficient to achieve significant phenol degradation, necessitating the addition of an exogenous oxidant.

Beyond this stoichiometric limitation, the specific reaction environment likely imposes additional kinetic constraints. While the in-situ generation of H_2O_2 is thermodynamically possible, its efficiency relies on Proton-Coupled Electron Transfer mechanisms, which are reported to be less effective when the water content is too low.[26] [27] In such a "water-starved" adsorption layer, the restricted proton mobility may favor charge carrier recombination making the production of oxidizing species less efficient.[28]. Consequently, the introduction of exogenous H_2O_2 serves as a strategic workaround to bypass these bottlenecks. In this system, H_2O_2 acts as a direct and highly efficient source of hydroxyl radicals ($HO\cdot$), which are the primary active species driving the rapid oxidative degradation of phenol.[29,30]

To implement this strategy while avoiding surface saturation or radical scavenging effects often associated with massive oxidant variability, a sequential "fed-batch" protocol was adopted. One molar equivalent of H_2O_2 (relative to phenol,

introduced via a 30% w/w solution) was added every 15 minutes following an initial 15 minutes dark equilibration period. Even accounting for the cumulative addition of the oxidative solution over the 120 minutes reaction time, the liquid-to-solid ratio (η) remains consistently within the range of $0.02 \leq \eta \leq 0.16$ $\mu L \cdot mg^{-1}$. This confirms that the reaction proceeds strictly under the Low-LAG regime, avoiding any transition to a slurry state that could alter the frictional energy transfer.

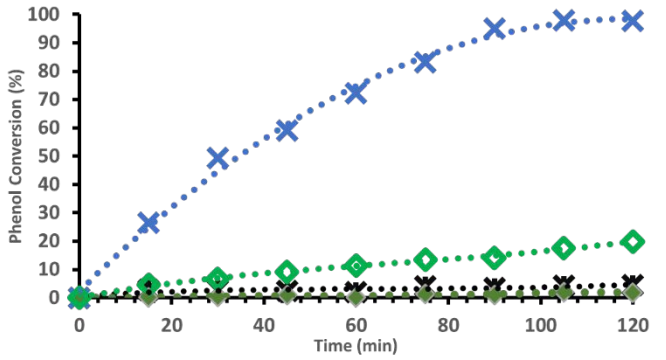

Fig. 1 : Phenol conversion over time in the presence of TiO_2 (1✱) in aqueous suspension in the dark; (2X) in aqueous suspension under UV irradiation; (5◆) under mechanochemical LAG conditions in the dark; (6◇) under photomechanochemical LAG conditions. (Phenol conversion was determined by NMR^1H).

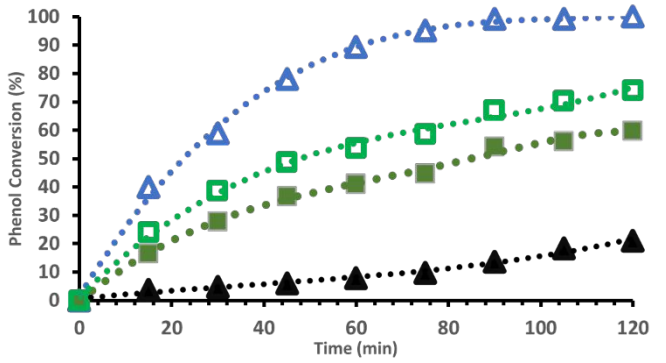

Fig. 2 : Phenol conversion over time in the presence of TiO_2 and H_2O_2 (7▲) in aqueous suspension in the dark; (8△) in aqueous suspension under UV irradiation; (9□) under mechanochemical LAG conditions in the dark; (10□) under photomechanochemical LAG conditions. (Phenol conversion was determined by NMR^1H).

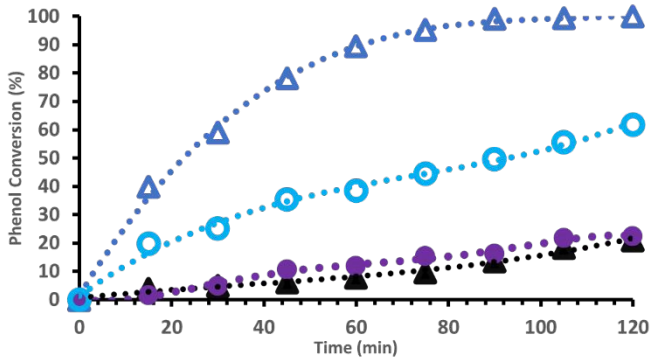

Fig 3: Phenol conversion over time in the presence of H_2O_2 in aqueous solution (7△) with pristine P25 under UV irradiation; (8○) with milled P25 under UV irradiation; (13□) with milled P25 in the dark; (14▲) and with pristine P25 in the dark. (Phenol conversion was determined by NMR^1H).

In aqueous suspension, the activation of the TiO_2/H_2O_2 system is predominantly governed by light irradiation, although a low reactivity exists in the dark. The non-irradiated control exhibits a slow but non-negligible phenol abatement, reaching 21% conversion after 120 minutes with a low associated kinetic constant is $k=1.64\times10^{-3}$ min^{-1}(Table 1. entry 7), reflecting limited surface interactions or minor chemical oxidation by H_2O_2 in the absence of photonic excitation. In stark contrast, UV irradiation triggers a drastic kinetic acceleration. The phenol conversion reaches >99% within 90 minutes, following a robust pseudo-first-order kinetics with a rate constant of $k=44.94\times10^{-3}$ min^{-1}(Table 1. Entry 8). This 27-fold increase in the reaction rate confirms that the mechanism is primarily photocatalytic: incident photons excite valence band electrons, which are efficiently scavenged by H_2O_2 to generate a high flux of hydroxyl radicals (HO·) responsible for the rapid attack on the aromatic ring.

Mechanochemical activation elicits a reactivity distinct from solution-based systems. (Fig 2) Most notably, the system exhibits substantial catalytic activity even in the complete absence of photonic irradiation. Under these dark conditions, phenol conversion reaches 54% within 90 minutes, following pseudo-first-order kinetics with a rate constant of $k=8.43\times10^{-3}$ min^{-1}(Table 1, Entry 9).

This result substantiates that the mechanical energy supplied by milling is sufficient to drive the oxidative degradation of the pollutant in the presence of H_2O_2, effectively substituting for the photonic excitation required in the aqueous suspension system. The concomitant application of UV irradiation and mechanochemical activation further enhances the overall performance, elevating the conversion to 67% at 90 minutes. The kinetic analysis reveals a rate constant increase to $k=12.33\times10^{-3}$ min^{-1}(Table 1, Entry 10). Although the relative rate enhancement factor (≈1.5) is markedly lower than the 27-fold surge observed in aqueous suspension, this positive increment points towards a degree of functional complementarity. It is plausible that photonic excitation and mechanical polarization operate cooperatively rather than competitively, with incident photons acting upon the available exposed surfaces while mechanical forces continuously modify and activate the inter-particle contacts.

To distinguish the transient effects of in-situ mechanical excitation from permanent structural modifications, catalytic tests were performed in aqueous suspension using P25 powder pre-activated by 120 minutes of milling. This ex-situ approach evaluates the reactivity of the processed material in the absence of mechanical stimuli. In the absence of H_2O_2 and UV irradiation, the pre-milled catalyst remains inert (Table 1, Entry 11). Under UV irradiation alone, a moderate activity is observed with a rate constant of $k=5.65\times10^{-3}$ min^{-1}(Table 1., Entry 12).

The introduction of H_2O_2 in the dark yields a kinetic constant of $k=2.18\times10^{-3}$ min^{-1}(Table 1, Entry 13). This value represents a 1.3-fold increase compared to the P25 evaluated under identical conditions with $k=1.64\times10^{-3}$ min^{-1} (Table 1, Entry 7). This small effect suggests that the mechanical pre-treatment likely induces structural modifications at the surface, potentially

View Article Online DOI: 10.1039/D6MR00074C

creating active sites capable of initiating H_2O_2 decomposition in the absence of light.

When subjected to UV irradiation in the presence of H_2O_2, the pre-milled sample exhibits a rate constant of $k=8.00\times10^{-3}$ min^{-1}(Table 1, Entry 14). While this represents an improvement over the non-oxidative condition (Table 1, Entry 12), it constitutes a drastic reduction, approximately 5.6-fold, compared to the P25 system with $k=44.94\times10^{-3}$ min^{-1} (Table 1., Entry 8). These results highlight a functional divergence: the structural changes induced by milling slightly enhance the dark reactivity but significantly impair the photocatalytic efficiency under photon flux (Fig. 3).

To track the degradation pathway, all reactions were monitored by ^1H NMR spectroscopy in D_2O, performed either directly on the aqueous samples or via solvent extraction for the mechanochemical assays (ESI). The spectra reveal the formation of 1,4-benzoquinone and formic acid in very low quantities. Notably, other expected aromatic intermediates, such as catechol or resorcinol, are completely absent. This observation aligns with recent multiphase NMR studies on P25,[31] which demonstrate that while hydroquinone is the primary detectable intermediate, its accumulation remains minimal relative to the initial phenol concentration.[32] The absence of other intermediates can be explained by their dynamics at the catalyst interface: primary oxidation products are either generated in concentrations too low to be detected, or they are consumed almost instantaneously by Reactive Oxygen Species (ROS) within the restricted mobility "gel phase" near the catalyst surface. Rather than significantly accumulating in the bulk solution, these transient species undergo a rapid cascade of successive oxidation steps, leading to a probable and swift mineralization.

Evaluation of dominant reactive species and the role of TiO_2 under mechanochemical activation

To elucidate the contributions of electrons (e^-) and holes (h^+) to the phenol degradation mechanisms, particularly in mechanocatalysis and photomechanocatalysis, we employed tert-butanol (tBuOH) as an electron (e^-) scavenger[33] and ethylenediaminetetraacetic acid disodium salt (EDTA.2Na) as a hole (h^+) scavenger.[34]

In aqueous suspension with H_2O_2 under UV irradiation, adding tBuOH significantly decreases the kinetic rate constant from $k=44.94\times10^{-3}$ min^{-1} to $k=17.30\times10^{-3}$ min^{-1} (Table 1, Entries 8 and 16). In contrast, EDTA.2Na induces no inhibitory effect (Table 1, Entry 20). Similarly, during photomechanocatalysis, the addition of tBuOH causes a sharp drop in the rate constant from $k=12.33\times10^{-3}$ min^{-1} to $k=7.49\times10^{-3}$ min^{-1} (Table 1, Entries 10 and 18), whereas EDTA.2Na exhibits no inhibitory effect (Table 1, Entry 22). Although less pronounced, the effect of tBuOH under mechanocatalytic conditions reduces from $k=8.43\times10^{-3}$ min^{-1} to $k=5.88\times10^{-3}$ min^{-1} (Table 1, Entries 9 and 17), with EDTA.2Na showing no significant impact.

Thus, whether in solution, photomechanocatalysis, or mechanocatalysis, the direct oxidation of phenol by holes appears negligible. Instead, the degradation is driven by conduction band electrons, which reduce H_2O_2 to generate oxidizing hydroxyl radicals, which are subsequently scavenged by tBuOH.

To decouple the effects of mechanical impacts from those associated with TiO_2, we selected Al_2O_3 (neutral aluminium oxide, Brockmann I) as a non-photoactive at 365nm,[35] insulating material to evaluate purely mechanical contributions to phenol degradation. Consequently, we observed poor phenol degradation, whether in the absence of UV ($k=2.12\times10^{-3}$ min^{-1}, Table 1, Entry 23) or under UV irradiation ($k=2.54\times10^{-3}$ min^{-1}, Table 1, Entry 24). In aqueous suspension, Al_2O_3 exhibited no catalytic activity, whether under UV irradiation or in the dark (Table 1, Entries 26 and 27). Thus, mechanical energy alone, dissipated through friction and impact, contributes only marginally to the homolytic cleavage of H_2O_2 into radicals without a redox-active catalyst.

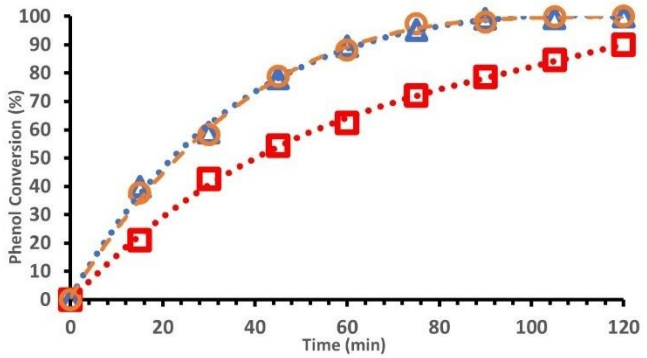

Fig. 4 : Phenol conversion over time in the presence of TiO_2 and H_2O_2 in aqueous suspension under UV irradiation (8△) without scavenger; (16○) with tBuOH electron scavenger; (20□) with EDTA.2Na hole scavenger. (Phenol conversion was determined by NMR^{1}H).

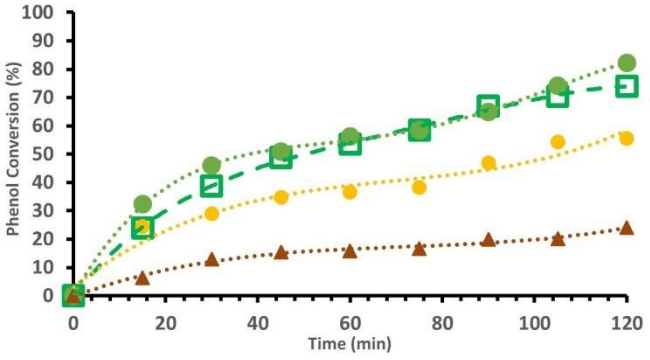

Fig. 5 : Phenol conversion over time in the presence of TiO_2 and H_2O_2 under mechanochemical LAG conditions with UV irradiation (10□) without scavenger; (16●) with tBuOH electron scavenger; (20●) with EDTA.2Na hole scavenger. Phenol conversion over time in the presence of Al_2O_3 and H_2O_2 under mechanochemical LAG conditions (13▲) with UV irradiation. (Phenol conversion was determined by NMR^{1}H).

View Article Online
DOI: 10.1039/D6MR00034G

Table 1. Pseudo-first-order kinetic rate constants (k) for phenol degradation.

Entry	Type	Catalyst	H_2O_2	tBuOH	EDTA.2Na	UV_{365nm}	$k(10^{-3}.min^{-1})$	R^2
1	Solution [a]	P25	no	no	no	no	n.d.	-
2	Solution [a]	P25	no	no	no	yes	30.09	0.955
3	Dry-Grinding [b]	P25	no	no	no	no	n.d.	-
4	Dry-Grinding [b]	P25	no	no	no	yes	n.d.	-
5	LAG-Grinding [c]	P25	no	no	no	no	n.d.	-
6	LAG-Grinding [c]	P25	no	no	no	yes	1.88	0.991
7	Solution [a]	P25	yes	no	no	no	1.64	0.977
8	Solution [a]	P25	yes	no	no	yes	44.94	0.978
9	LAG-Grinding [d]	P25	yes	no	no	no	8.43	0.991
10	LAG-Grinding [d]	P25	yes	no	no	yes	12.33	0.991
11	Solution [e]	Ball-milled P25	no	no	no	no	n.d.	-
12	Solution [e]	Ball-milled P25	no	no	no	yes	5.65	0.994
13	Solution [e]	Ball-milled P25	yes	no	no	no	2.18	0.990
14	Solution [e]	Ball-milled P25	yes	no	no	yes	8.00	0.990
15	Solution [a]	P25	yes	yes	no	no	0.55	0.939
16	Solution [a]	P25	yes	yes	no	yes	17.30	0.999
17	LAG-Grinding [d]	P25	yes	yes	no	no	5.88	0.973
18	LAG-Grinding [d]	P25	yes	yes	no	yes	7.49	0.968
19	Solution [a]	P25	yes	no	yes	no	1.49	0.981
20	Solution [a]	P25	yes	no	yes	yes	47.83	0.961
21	LAG-Grinding [d]	P25	yes	no	yes	no	7.37	0.944
22	LAG-Grinding [d]	P25	yes	no	yes	yes	12.94	0.976
23	LAG-Grinding [d]	Al_2O_3	yes	no	no	no	2.12	0.947
24	LAG-Grinding [d]	Al_2O_3	yes	no	no	yes	2.54	0.955
25	Solution [a]	Al_2O_3	yes	no	no	no	n.d.	-
26	Solution [a]	Al_2O_3	yes	no	no	no	n.d.	-
27	LAG-Grinding [d]	Reused P25	yes	no	no	no	3.99	0.993
28	LAG-Grinding [d]	Reused P25	yes	no	no	yes	10.37	0.981

a: 10 mL of phenol solution at 10 $mg.L^{-1}$; 5 mg of P25 or Al_2O_3 (catalyst to phenol mass ratio = 50); 0 eq. or 1 eq. of H_2O_2 (in water solution at 30 %w/w) every 15 min ; 0eq. or 1 eq. of tBuOH every 15 min; 0 eq. or 1 eq. of EDTA.2Na every 15 min; UV_{365nm} 0 $mW.cm^{-2}$ or 3 $mW.cm^{-2}$

b: 80 mg of phenol; 4000 mg of P25 (catalyst to phenol mass ratio = 50); UV_{365nm} 0 $mW.cm^{-2}$ or 3 $mW.cm^{-2}$

c: 80 mg of phenol; 4000 mg of P25 (catalyst to phenol mass ratio = 50); 80uL of H_2O every 15 min; UV_{365nm} 0 $mW.cm^{-2}$ or 3 $mW.cm^{-2}$

d: 80 mg of phenol; 4000 mg of P25 or Al_2O_3 (catalyst to phenol mass ratio = 50); 0 eq. or 1 eq. of H_2O_2 (in water solution at 30%w/w) every 15 min; 0 eq. or 1 eq. of tBuOH every 15 min; 0 eq. or 1 eq. of EDTA.2Na every 15 min; UV_{365nm} 0 $mW.cm^{-2}$ or 3$mW.cm^{-2}$

e: 10 mL of phenol solution at 10 $mg.L^{-1}$; 5mg Ballmilled P25 (catalyst to phenol mass ratio = 50); 0 eq. or 1 eq. of H_2O_2 every 15 min; UV_{365nm} 0 $mW.cm^{-2}$ or 3 $mW.cm^{-2}$

Structural and morphological stability and modifications of TiO2 under mechanical stress

Having observed the distinct impact of mechanical stress on the final phenol conversions, a functional trade-off is clearly evidenced. In an aqueous suspension with H_2O_2, pristine P25 achieves >99% conversion under UV irradiation within 90 minutes but only yields 21% in the dark after 120 minutes. The pre-milled catalyst maintains a similar dark activity of 22% at 120 minutes, yet it suffers a drastic photocatalytic collapse to 62% under UV. Furthermore, the in situ mechanochemical system demonstrates a remarkable 60% conversion in the dark and 74% under simultaneous UV irradiation. To provide a mechanistic understanding of these complex catalytic behaviors, particularly the striking dark mechanochemical activation, the severe collapse of the pre-milled catalyst's photoefficiency in solution and the superior efficiency of the coupled photomechanochemical system, it is essential to correlate the kinetic data with the physicochemical evolution of the material. The observed reactivity suggests that vibratory milling induces fundamental alterations in the semiconductor's architecture. Consequently, a systematic characterization of the milled P25 was conducted to decouple the effects of textural reorganization (surface area, porosity) from intrinsic electronic modifications (band gap, defect density), thereby identifying the structural descriptors governing this mechano-responsive behavior.

The diffraction pattern of the P25 confirms the presence of characteristic crystalline phases, with a predominance of anatase (peak at 2θ=25.3∘, (101) plane) and a minor contribution from the rutile phase (peak at 2θ=27.4∘, (110) plane). Following mechanochemical treatment, no significant shift in peak positions nor alteration of their Full Width at Half Maximum (FWHM) is observed (Fig. 6). Application of the Scherrer equation[36] indicates that the average crystallite size remains unchanged with 18nm for anatase (based on peak at 2θ=25.3∘, (101) plane) and 26nm for rutile (based on peak at 2θ=27.4∘, (110) plane). Furthermore, the anatase/rutile phase ratio is preserved (80% anatase, 20% rutile), suggesting that the mechanical energy dissipated upon impact is insufficient to induce an allotropic phase transition or material amorphization under our operating conditions.

To further probe the local structural integrity, Raman spectroscopy was performed (Fig. 7). The spectra of the activated samples (15 and 120 min) overlap perfectly with that of P25 without grinding. Under our measurement conditions, the spectral features are dominated by the majority anatase phase, allowing the distinct observation of its six active modes (A1g+2B1g+3Eg)[37], notably the intense E_g mode at 144 cm^{-1}. The absence of any significant broadening or shifting confirms that the crystalline order is preserved even at the local scale,[38] and that the defects induced by milling are probably confined to the surface.

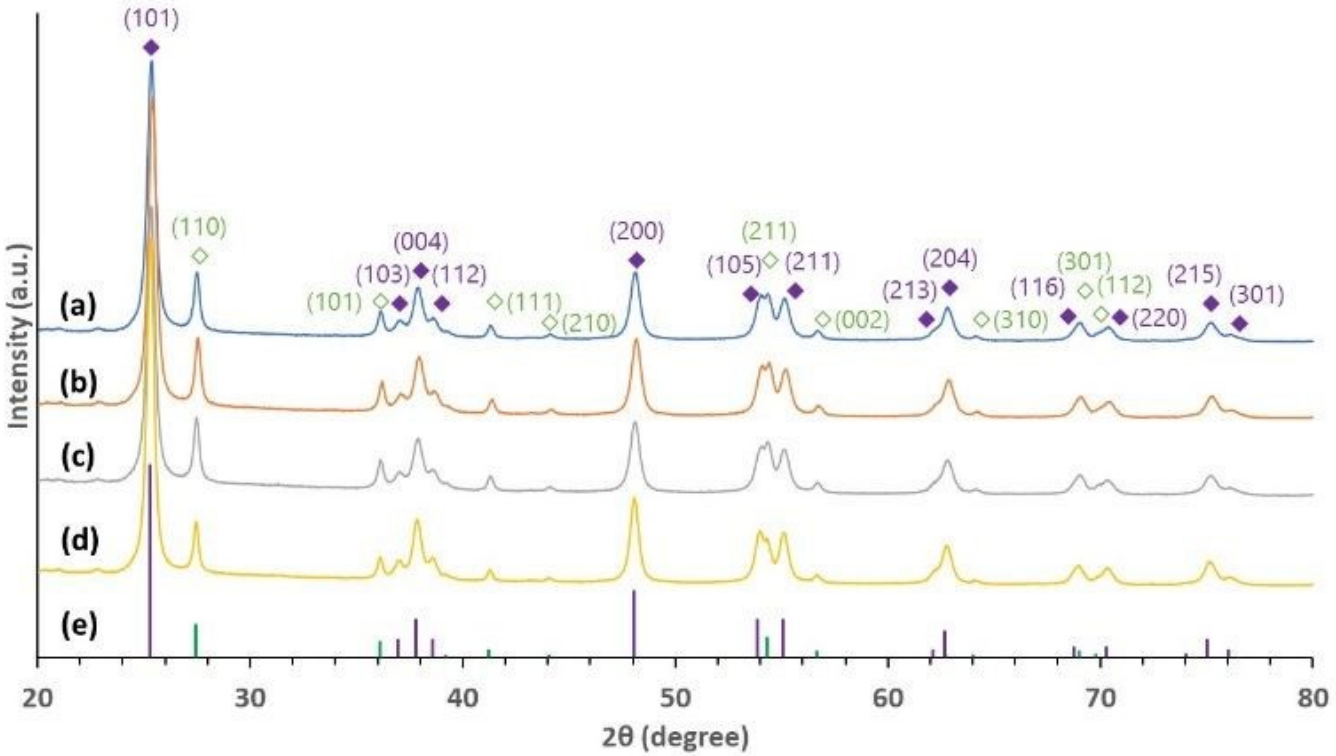

Fig. 6: XRD patterns of (a) pristine P25, (b) P25 milled at 20 Hz for 15 min, (c) P25 milled at 20 Hz for 120 min, and (d) P25 milled at 20 Hz for 120 min after catalytic evaluation. (e) theorical position of Bragg reflections associated to 80% of anatase and 20% of rutile. The remarked crystalline phases are the anatase (JCPDS 21-1272) (◆) and rutile (JCPDS 21-1276) (◇).

View Article Online
DOI: 10.1039/D6MR00034G

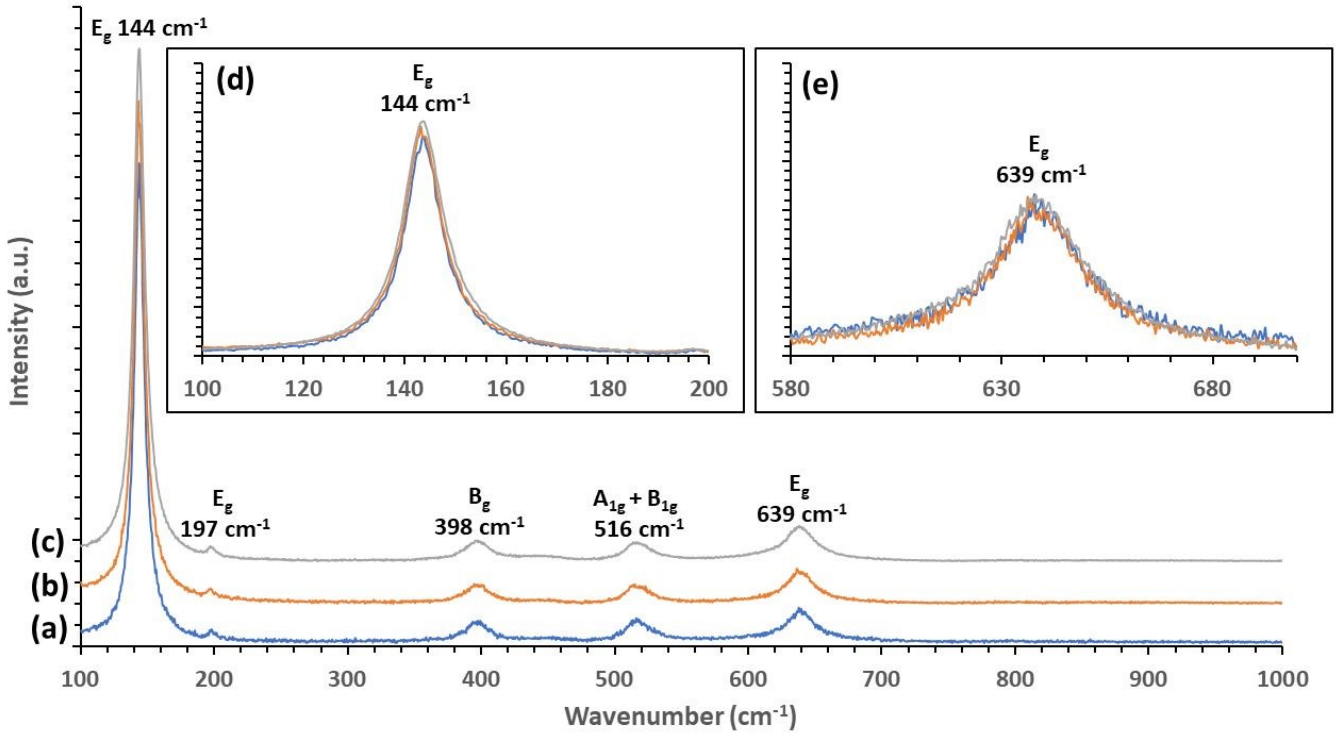

Fig.7 : Normalized Raman spectra (a) Pristine P25 (b) grinding P25 at 20 Hz for 15min (c) grinding P25 at 20 Hz for 120 min. Enlarged views of the (d) Eg mode at 144 cm^{-1} and (e) Eg mode at 639cm^{-1}.

The impact of milling on the textural properties of P25 was monitored via N_2 physisorption. The corresponding adsorption and desorption isotherms (Fig. 8a-b) exhibit Type IV behavior according to the IUPAC classification, characteristic of intergranular mesoporosity.[39] Data analysis reveals a remarkable stability of the specific surface area (SBET), which remains constant between 62 $m^2 g^{-1}$ and 63 $m^2 g^{-1}$ regardless of the treatment duration. This invariance indicates that the dissipated mechanical energy is insufficient to fracture the primary TiO_2 crystallites. However, an examination of the pore size distribution profiles (Fig. 8c) reveals significant morphological rearrangements at the aggregate level. While the overall pore volume remains comparable between the pristine P25 and the sample milled for 15 minutes, their distribution profiles present a notable divergence. Specifically, the pristine P25 possesses a higher proportion of small mesopores below 6 nm, whereas the briefly milled sample exhibits a distinct shift towards larger pore populations. Although the average pore size remains centred around 40 nm for both of these samples, this initial redistribution strongly suggests a rapid dispersion of the original agglomerates. From a structural perspective, this rapid evolution can be attributed to the mechanical cleavage of the anatase and rutile heterojunctions that originally architected these small cavities. The disruption of these critical inter-phase contacts leads to their disappearance in favor of larger inter-particle voids. Extending the milling treatment to 120 minutes induces a secondary textural evolution characterized by severe mechanical compaction. The average pore size drastically decreases to approximately 15 nm, effectively reducing the intergranular spacing without altering the intrinsic specific surface area of the individual grains. These textural evolutions are visually corroborated by electron microscopy imaging (Fig. 9). The micrographs depict the initial dispersion of the agglomerates during the early stages of milling followed by a pronounced structural compaction at the end of the treatment. This microscopic densification directly translates to the macroscopic scale, yielding a notably less pulverulent and more cohesive final powder.

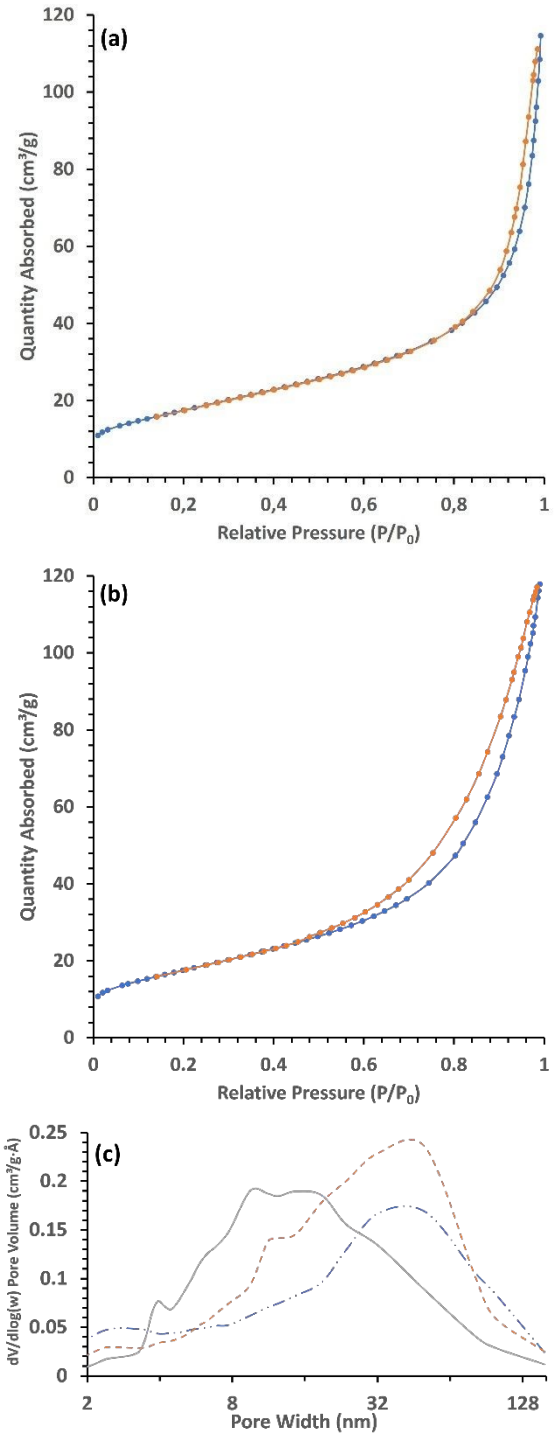

Fig. 8: N_2 adsorption-desorption isotherms of (a) pristine P25; (b) P25 milled at 20 Hz for 120 min; (c) Pore width distribution of (—··—) pristine P25, (- - -) P25 milled at 20Hz for 15 min and (—) P25 milled at 20Hz for 120 min

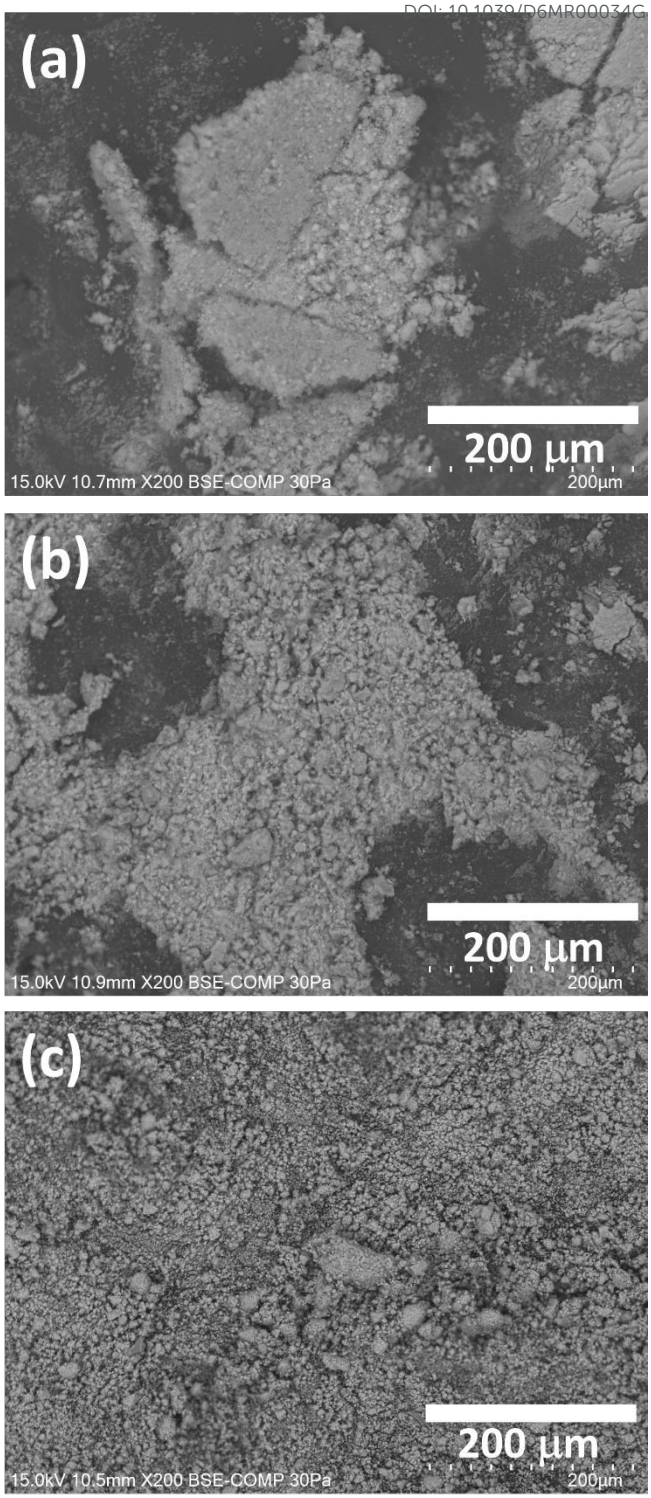

Fig.9: SEM micrographs of (a) pristine P25, (b) P25 milled at 20 Hz for 15 min, and (c) P25 milled at 20 Hz for 120 min.

The influence of mechanical activation on the electronic structure was investigated via Diffuse Reflectance Spectroscopy (DRS). The Kubelka-Munk transformed absorption spectra, F(R), are presented in Fig. 10a. A distinct red-shift of the absorption edge toward longer wavelengths is qualitatively observed as the milling duration increases, indicating enhanced absorption in the near-visible region. To quantify this evolution, optical band gap energies (E_g) were determined via Tauc plots[40] by plotting $[F(R)hv]^{1/2}$ as a function of photon energy (hv) (Fig. 10 b-d). Linear extrapolation of the absorption edge yields a value of 3.29 eV for P25 without grinding. This value decreases significantly to 3.16 eV after 15 min, reaching 3.02 eV after 120 min of activation. This 0.26 eV reduction in the optical gap, occurring without any crystalline phase transition, crystallite size alteration, or material amorphization as previously demonstrated by XRD, is attributed to the creation of mid-gap defect states induced by mechanical impacts. These localized energy levels, situated below the conduction band, facilitate electronic transitions at lower energies. To further elucidate the nature of these defects, the Urbach energy (E_u)[41] was determined from the exponential absorption tails (Fig. 10e-g).

The results reveal a non-linear evolution: a sharp increase from 47 meV for P25 without grinding to 59 meV occurs within the first 15 minutes, followed by a plateau-like stabilization at 63 meV after 120 min. In P25, defects are known to be predominantly localized at the interfacial contacts between anatase and rutile crystallites. Consequently, the initial surge in Eu is attributed to the mechanical disruption of these inter-phase heterojunctions during the rapid de-agglomeration stage, which exposes a high density of localized states. The subsequent stabilization of E_u suggests that once these primary junctions are decoupled, prolonged milling proceeds via surface friction, generating fewer additional structural distortions. Given that the bulk crystallinity remains invariant (Fig. 4), this evolution confirms that the band gap narrowing is driven by a surface-confined phenomenon linked to the mechanical breakdown of the nanoparticle network. The milling facilitates the formation of oxygen vacancies and reduced titanium centers (Ti^{n+}), which generate the localized electronic levels responsible for the observed band-tail broadening.[42]

This multi-scale characterization demonstrates that mechanical activation drives a significant electronic and textural surface reorganization, manifested by band gap narrowing and pore network evolution, while strictly maintaining bulk crystalline integrity. Consequently, the processed catalyst behaves as a surface-activated material, where the structurally intact anatase and rutile crystallites simply exhibit a defective surface.

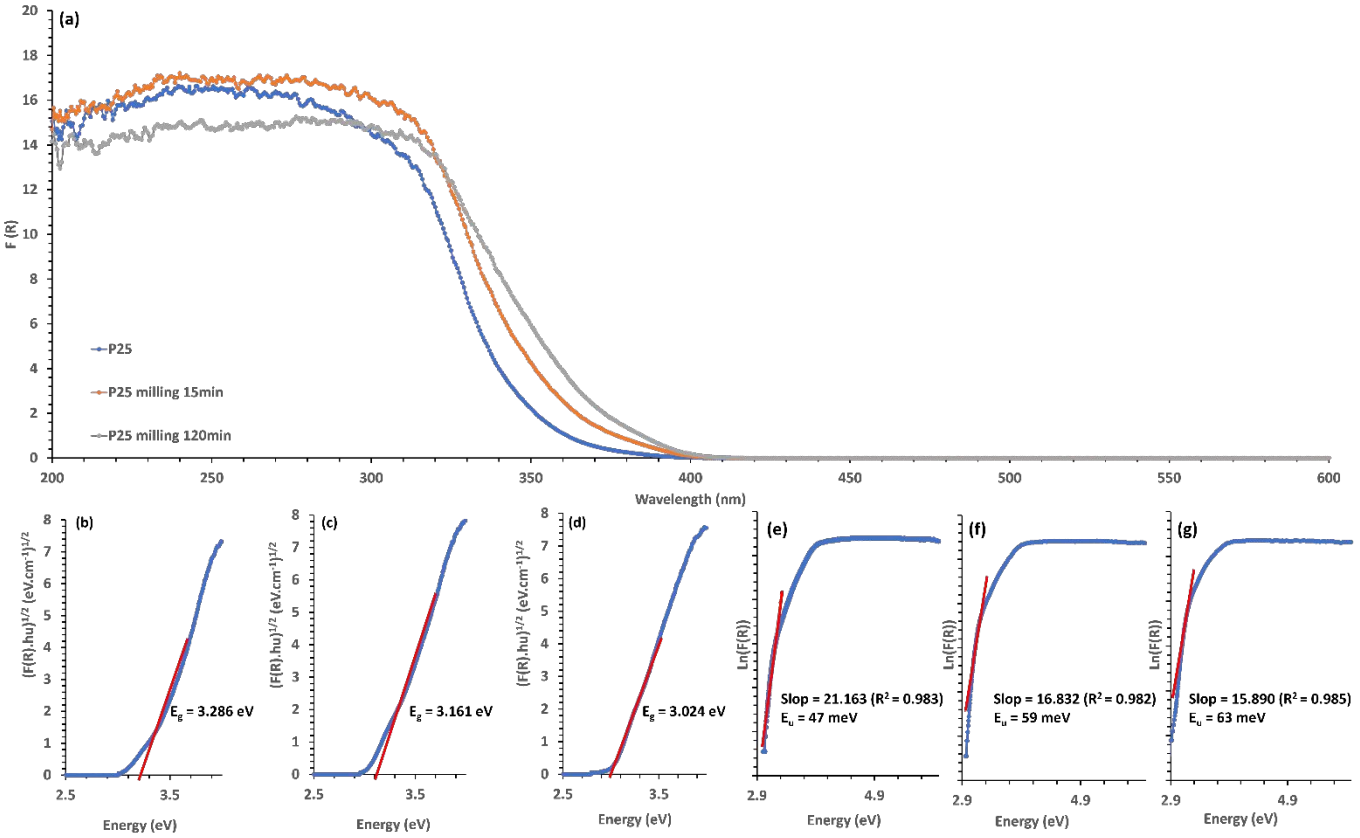

Fig.10: (a) Kubelka-Munk transformed diffuse reflectance spectra and corresponding Tauc plots for (b) pristine P25, (c) P25 milled at 20 Hz for 15 min, and (d) P25 milled at 20 Hz for 120 min. Urbach energy determination from the ln[F(R)] vs. photon energy plots for (e) pristine P25, (f) P25 milled at 20 Hz for 15 min, and (g) P25 milled at 20 Hz for 120 min.

View Article Online
DOI: 10.1039/D6MR00034G

Mechanistic correlation between structural disruption and the functional trade-off in photomechanocatalysis

The catalytic performance in classical aqueous suspension relies on the architecture of the P25 photocatalyst. This material is a complex assembly of aggregates where anatase and rutile nanocrystallites are connected by solid heterojunctions, recognized for optimizing charge separation under irradiation. In this context, mechanochemical activation acts as a disruption process where the shear energy imposed by vibratory milling fractures the inter-particle cohesion zones, dissociating the initial aggregates. This mechanical action induces a major beneficial effect for dark activation. The scission of Ti–O–Ti bridges at the interfaces generates a population of active surface defects, identified by the rise in Urbach energy (E_u). We postulate that these localized sites, potentially comprising reduced metallic centers (Ti^{n+}) and oxygen vacancies, could possess sufficient electrochemical potential to spontaneously interact with H_2O_2. They might therefore serve as chemical initiation centers to enable hydroxyl radical (·OH) production and phenol degradation in the absence of light. Thus, the disruption of these crystalline junctions appears to be the main driving force behind the pure mechanochemical reactivity. However, this restructuring imposes a functional trade-off under UV irradiation. The efficiency of P25 in aqueous suspension relies on the integrity of the anatase-rutile heterojunctions, which serve as separation sinks for electron-hole pairs (e^-/h^+). The partial breakdown of these intimate contacts during milling alters this synergistic mechanism. By dissociating the phases, the mechanical treatment isolates a portion of the crystallites, potentially favoring the immediate recombination of photogenerated charges at the expense of their transfer to the surface (Fig. 11B). This structural alteration rationalizes why the UV kinetics in photomechanochemistry remain lower than those observed in an aqueous suspension.

The system thus exists in a state of reactive compromise where the input of mechanical energy sacrifices a portion of the optimal photocatalytic architecture through the cleavage of heterojunctions. This sacrifice generates a new surface reactivity that allows the system to operate under dark conditions where the intact photocatalyst would be entirely inoperative.

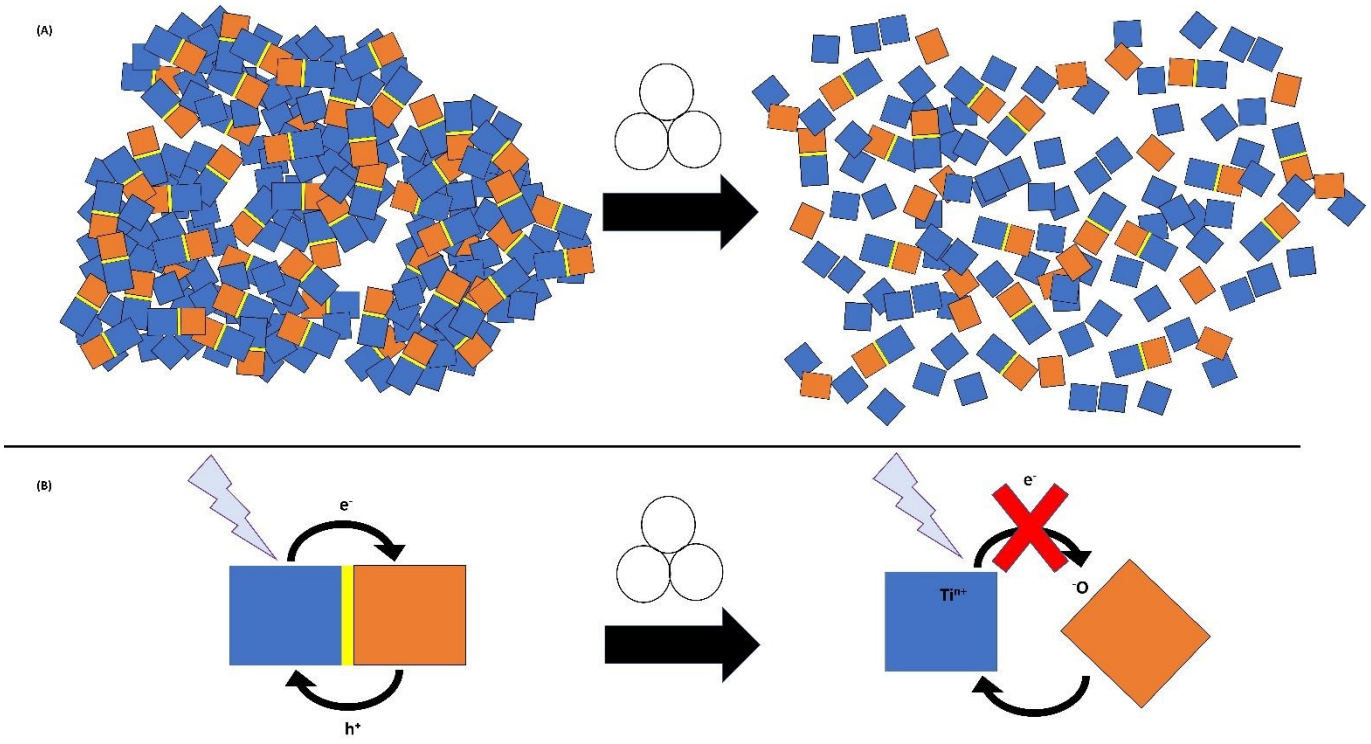

Fig. 11: (A) Schematic representation of the structural disruption of P25 aggregates under vibratory milling, illustrating the physical cleavage of anatase-rutile heterojunctions (Anatase-rutile: blue-orange; heterojunction: yellow). (B) Schematic illustration of the resulting inhibition of interphase charge transfer with physical dissociation of anatase-rutile interfaces inherently prevents the synergistic separation of photogenerated electrons (e^-) and holes (h^+).

View Article Online
DOI: 10.1039/D6MR00034G

Table 2. Green metrics at 120 min reaction time.

Entry	Type	K[e] (10^{-3}.min^{-1})	Phenol removed (%)	GMI[f] (10^{-3} g/g)	PMI[g]	Modified E-factor[h]
1	UV H_2O P25 Solution [a]	30.09	98	0.978	102298	102297
2	UV P25 LAG-H_2O Grinding [b]	1.88	20	335	299	298
3	Dark P25 H_2O_2 Solution [a]	1.64	21	0.209	478230	478215
4	UV P25 H_2O_2 Solution [a]	44.94	100	0.999	100061	100057
5	Dark P25 LAG-H_2O_2 Grinding [c]	8.43	60	986	101	96
6	UV P25 LAG-H_2O_2 Grinding [c]	12.33	74	1220	82	77
7	UV H_2O grinded P25 Solution [d]	5.65	48	0.483	207078	207077
8	Dark H_2O_2 grinded P25 Solution [d]	2.18	22	0.224	446473	446459
9	UV H_2O_2 grinded P25 Solution [d]	8.00	62	0.619	161664	161658

a: 10mL of phenol solution at 10 mg.L^{-1}; 5 mg of P25 (catalyst to phenol mass ratio = 50); 0 eq. or 1 eq. of H_2O_2 (in water solution at 30 %w/w) every 15 min; UV_{365nm} 0 mW.cm^{-2} or 3 mW.cm^{-2}
b: 80 mg of phenol; 4000 mg of P25 (catalyst to phenol mass ratio = 50); 80uL of H_2O every 15 min; UV_{365nm} 0 mW.cm^{-2} or 3 mW.cm^{-2}
c: 80 mg of phenol; 4000 mg of P25 (catalyst to phenol mass ratio = 50); 0 eq. or 1 eq. of H_2O_2 (in water solution at 30 %w/w) every 15 min; UV_{365nm} 0 mW.cm^{-2} or 3mW.cm^{-2}
d: 10 mL of phenol solution at 10mg.L^{-1}; 5 mg Ballmilled P25 (catalyst to phenol mass ratio= 50); 0 eq. or 1 eq. of H_2O_2 every 15 min; UV_{365nm} 0 mW.cm^{-2} or 3 mW.cm^{-2}
e: Pseudo-first-order kinetic rate constants
f: Global Material Economy; GMI = (mass of phenol removed) / (total mass used in process)
g: Process mass intensity, PMI = ((Total mass in process) / (mass of phenol removed)) x 100
h: Modified E-factor = ((total mass in process) – (mass of phenol removed)) / (mass of phenol removed)

Catalyst reusability

To evaluate the reusability of P25 after a first 120-minute mechanocatalytic cycle, a sequential replenishment strategy was employed. Specifically, the phenol conversion at 120 minutes was quantified in order to accurately recharge the milling jar with phenol, thereby rigorously maintaining the initial catalyst-to-pollutant mass ratio at R=50 for the subsequent run.

The kinetic evaluation of this second cycle provides insights into the possible nature of the mechanically generated active sites. Under dark mechanochemical conditions, a deactivation is observed, with the pseudo-first-order rate constant decreasing from $k=8.43\times10^{-3}$ min^{-1} in the first run (Table 1, Entry 9) to $k=3.99\times10^{-3}$ min^{-1} in the second run (Table 1, Entry 27). This loss of dark activity is consistent with the proposed mechanistic model where the spontaneous, light-independent reactivity is driven by surface defects created during the initial fracturing of the anatase-rutile agglomerates. Over the course of the reaction, these surface states are oxidized and passivated by H_2O_2. Because the primary heterojunctions are largely cleaved after the first run, the subsequent milling of the dispersed particles generates fewer new structural defects, resulting in a depleted pool of active initiation sites for the dark reaction.

Conversely, when the mechanochemical recycling is coupled with UV irradiation, the catalytic performance is maintained. The pseudo-first-order rate constant shows a minor decrease, shifting from $k=12.33\times10^{-3}$ min^{-1} to $k=10.37\times10^{-3}$ min^{-1} (Table 1, Entries 10 and 28). This retention of activity under UV irradiation indicates that while the transient surface defects generated by heterojunction deconstruction are reoxidized and passivated by H_2O_2 over time, the intrinsic photocatalytic properties of the material remain operational. Despite the prolonged mechanical stress, the semiconductor retains its capacity to generate electron-hole pairs upon UV absorption, allowing the TiO_2 to be effectively reused for this new photomechanocatalytic cycle.

However, continuing this recycling protocol is hindered by a rheological limitation. The sequential addition of the aqueous H_2O_2 solution inevitably increases the liquid-to-solid ratio (η) over successive cycles. While the first 120 minutes cycle operated under a strictly controlled low-LAG regime ($0.02\leq\eta\leq0.16$ µL.mg^{-1}), the second cycle reached higher values between 0.16 µL.mg^{-1} and 0.32 µL.mg^{-1}. Upon the final addition, a major macroscopic modification was observed, characterized by significant agglomeration of the powder bed. This physical state precludes maintaining comparable mixing dynamics, rendering a third 120 minutes cycle under identical experimental conditions unfeasible. Although a conventional catalyst recycling procedure involving washing and drying steps is technically possible, this approach was deliberately discarded. Such a treatment would generate substantial solvent

volumes, directly penalizing the green chemistry metrics targeted by this process, especially for a low-cost benchmark material like P25. This decision is further supported by the functional assessment of the material with a marked passivation in dark mechanocatalysis contrasting with the retention of its properties under UV irradiation. Consequently, future research should pursue two main directions, with the development of more efficient photoactive materials tailored for photomechanocatalysis and by the design of catalysts specifically engineered for dark mechanocatalysis, capable of continuously regenerating their active surface sites under continuous friction and impact.

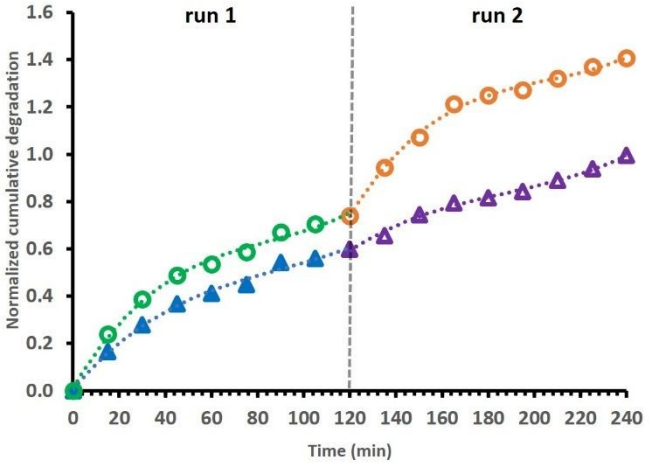

Fig. 12 : Cumulative degradation of phenol over time in the presence of TiO_2 and H_2O_2 under photomechanochemical LAG conditions (○) run 1 and (○) run2 or, under photomechanochemical LAG conditions (▲) run 1 and (△) run2. (Phenol conversion was determined by NMR ^1H, normalized cumulative degradation represents the total amount of phenol oxidized across successive cycles relative to the initial phenol loading).

Quantitative environmental assessment via green chemistry metrics

To rigorously assess the environmental pertinence of transitioning from classical solution-based photocatalysis to mechanochemical activation, specific green chemistry metrics, Global Material Economy (GME),[43] Process Mass Intensity (PMI), and a modified E-factor, were quantified[44] (Table 2). To accurately reflect the remediation process, the E-factor was specifically adapted to track the mass of the removed pollutant rather than a synthesized product. This modified metric is calculated as follows Modified E-factor with:

$$Modified\ E.factor = \frac{\text{total mass in process} - \text{mass of phenol removed}}{\text{mass of phenol removed}}$$

This practical adaptation provides a direct and realistic evaluation of the depollution efficiency.

These mass-based indicators are particularly relevant for this study as they heavily penalize the use of bulk auxiliary liquids, providing a transparent evaluation of whether the material efficiency gained by operating in a nearly solvent-free environment genuinely offsets any potential kinetic compromises. When analysing these metrics, establishing a direct baseline comparison with the pristine catalyst in aqueous solution under dark conditions (Table 2, Entry 3) lacks practical relevance. Under these conditions, the system achieves a modest 21% phenol removal after 120 min, rendering its exceedingly high E-factor of 478215 reflective of a severely limited process rather than a viable remediation standard. The true environmental viability of the mechanochemical approach must be evaluated against the optimal solution-based benchmark which is the P25 under UV irradiation with H_2O_2 (Table 2, Entry 4), which achieves 100% phenol removal with an E-factor of 100057. Against this highly active baseline, the transition to the low-LAG regime demonstrates a transformative improvement. Remarkably, even in the complete absence of UV irradiation, the mechanochemical process (Table 2, Entry 5) achieves a highly significant 60% phenol removal, drastically slashing the E-factor to a low value of 96. When mechanical activation is concomitantly coupled with UV irradiation (Table 2, Entry 6), the phenol removal increases to 74%, and the E-factor is further optimized, decreasing to 77. This represents a staggering 1299-fold improvement compared to the optimal aqueous system (Entry 8). The drastic leap in GME (Fig. 13) and the concomitant collapse of the PMI underscore that the physical elimination of the bulk water reservoir is the absolute driver of the system's green credentials. Conversely, evaluating the pre-milled P25 back in a classical aqueous suspension provides a stark quantitative translation of the previously discussed functional trade-off. Under UV irradiation, the structural disruption of the anatase-rutile heterojunctions severely degrades the reaction's efficiency. The milled catalyst (Table 2, Entry 9) only achieves 62% phenol removal, exhibiting a 1.6-fold degradation in the E-factor compared to the intact P25 (161658 vs. 100057; Table 2, Entries 9 and 4), coupled with a proportional degradation in PMI.

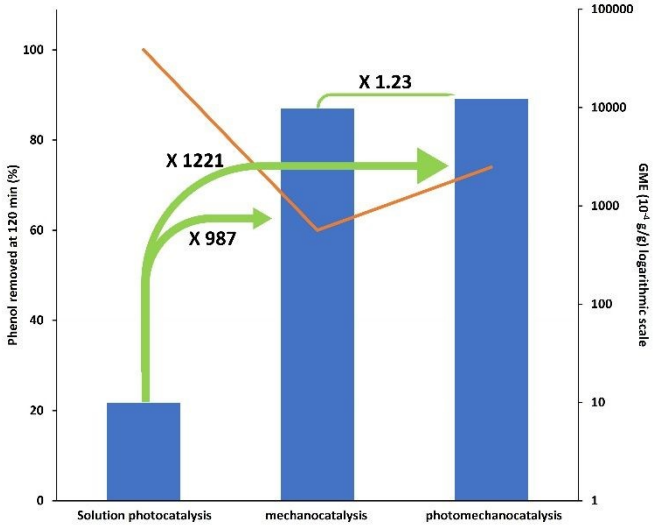

Fig. 13: Global Material Economy evolution and Proportion of phenol removed at 120min; ***Solution photocatalysis:*** 10mL of phenol solution at 10mg.L^{-1}; 5mg of P25 (catalyst to phenol mass ratio = 50); 0 eq. or 1 eq. of H_2O_2 (in water solution at 30%w/w) every 15 min; UV_{365nm} 3 mW.cm^{-2} ; ***mechanocatalysis:*** 80 mg of phenol; 4000mg of P25 (catalyst to phenol mass ratio = 50); 0 eq. or 1 eq. of H_2O_2 (in water solution at 30%w/w) every 15 min; UV_{365nm} 0 mW.cm^{-2}; ***photomechanocatalysis:*** same condition of 9 with UV_{365nm} 3 mW.cm^{-2} .

Conclusions

In conclusion, this study establishes the viability of coupling mechanical activation with UV irradiation for the remediation of organic pollutants, using phenol degradation over P25 TiO_2 as a model benchmark. Operating under a strictly controlled low liquid-assisted grinding (LAG) regime with the sequential addition of H_2O_2, results demonstrate that mechanical energy can initiate oxidative degradation in the absence of light. Multiscale characterization demonstrates that the vibratory milling process induces a critical structural disruption at the aggregate level. While the bulk crystalline integrity is preserved, the evolutions strongly suggest the fragmentation of the initial anatase-rutile heterojunctions. This physical deconstruction generates a defective surface layer leading to an optical band gap narrowing to 3.02 eV where these defects serve as chemical initiation sites capable of spontaneously activating H_2O_2 independently of photonic flux.

However, this investigation exposes a functional trade-off inherent to photomechanocatalysis. While the cleavage of inter-phase heterojunctions is essential for initiating dark mechanocatalytic activity, it simultaneously compromises the separation of photogenerated charge carriers (e^-/h^+) required for optimal UV photocatalysis. Consequently, the milled P25 operates in a state of reactive compromise, where the gain in dark reactivity occurs at the expense of the material's intrinsic photonic efficiency. This phenomenon is further compounded by the transient nature of the mechanically induced surface sites. Reusability tests show that these active centers are progressively reoxidized and passivated by H_2O_2 over time, resulting in a significant decrease in the kinetic rate constant during subsequent dark cycles, where k drops from 8.43×10^{-3} min^{-1} to 3.99×10^{-3} min^{-1}. Conversely, the photocatalytic properties remain operational under UV irradiation, confirming that the semiconductor retains its capacity to generate electron-hole pairs despite prolonged mechanical stress.

Beyond kinetic considerations, the quantitative assessment via green chemistry metrics underscores the environmental relevance of this approach. Despite the observed kinetic compromises, transitioning to a nearly solvent-free environment facilitates a transformative improvement in the Global Material Economy (GME) and a massive reduction in the modified E-factor compared to traditional aqueous suspensions.

Ultimately, these findings broaden the application of mechanochemistry to water-starved environmental remediation and suggest a new roadmap for materials science. Future catalyst design for photomechanocatalysis must address this reactive compromise through targeted architectural engineering. To limit the degradation of photonic efficiency, next-generation materials must be capable of maintaining efficient electron-hole separation under severe mechanical stress. This could be achieved through resilient internal architectures or robust core-shell geometries capable of withstanding high-shear environments. Concurrently, to overcome the rapid passivation of transient catalytic centers, the external surfaces of these materials must be specifically designed for facilitate the continuous exposure of fresh, highly reactive surfaces, catalysts could persistently regenerate active redox sites under constant friction and impact. Reconciling these opposing requirements what are bulk structural durability for sustained charge separation and surface mechanosensitivity for continuous active site generation will be the critical challenge for developing truly synergistic dual-activated environmental catalysts.

Author contributions

Conceptualization SM; methodology, validation, investigation, resources, data curation, GD, AP, SM; formal analysis: GD, NK; writing original draw preparation, SM; writing review and editing, GD, NK, AP, SM; supervision, AP, SM; project administration, SM, AP; funding acquisition, SM.

Conflicts of interest

There are no conflicts to declare.

Data availability

All data supporting this study are available within the article and it associated Electronic Supplementary Information (ESI) file. Any additional data related to this work are available from the corresponding author upon reasonable request.

Acknowledgements

The authors further extend they are thanks to France 2030 for major funding the ECOCHEM (ANR-22-PESP-0006) and the University of Artois within which this study was carried out. The authors acknowledge the Chevreul Institute (FR 2638) and the CPER ECRIN program, supported by the Hauts-de-France Regional Council, the French Ministry of Higher Education and Research, and the European Regional Development Fund, for their partial financial support of this work. Pr. Sébastien Saitzek, Pr. Jean-François Blach and Dr. Marie-Hélène Chambrier are acknowledged for RAMAN et XRD access. Dr. Jérémy Ternel is acknowledged for providing NMR access, and the CPER research project BiHauts Eco de France is recognized for funding the acquisition of the Bruker AVANCE NEO 400 spectrometer.

Notes and references

View Article Online
DOI: 10.1039/D6MR00034G

[1] K. F. Alshammari, Luminescence, 2024, 39, e4808.

[2] A. K. Moharana and R. Vaish, J. Appl. Phys., 2025, 138, 135002.

[3] H. Sudrajat, H.-Y. Hsu and J. C. Colmenares, J. Mater. Chem. A, 2025, 13, 27925–27946

[4] Y. He, Z. Jin, S. Wu, C. Jiang, C. Hu and L. Liu, ACS Omega, 2025, 10, 32339–32347.

[5] X. Cui, P. Li, H. Lei, C. Tu, D. Wang, Z. Wang and W. Chen, Sep. Purif. Technol., 2022, 289, 120814.

[6] Y. Du, S. Zhang and Z. Cheng, Nano Energy, 2024, 127, 109731.

[7] Y. Zhang, Z. Wu, L. Zhang, C. Cheng, H. Yi, R. Yan, Z. Wu, Y. Wang, X. Shi, G. Yao, G. Zhu and Y. Jia, J. Alloys Compd., 2025, 1014, 178654.

[8]M.C. Cotto, A. Emiliano, S. Nieto, J. Duconge and R. Roque-Malherbe , J. Colloid Interface Sci., 2009, 339, 133–139

[9] S. L. James, C. J. Adams, C. Bolm, D. Braga, P. Collier, T. Friščić, F. Grepioni, K. D. M. Harris, G. Hyett, W. Jones, A. Krebs, J. Mack, L. Maini, A. G. Orpen, I. P. Parkin, W. C. Shearouse, J. W. Steed and D. C. Waddell, *Chem. Soc. Rev.*, 2012, **41**, 413-447

[10] N. Shan, F. Toda and W. Jones, *Chem. Commun.*, 2002, 2372–2373

[11] K. Cousin, S. Menuel, E. Monflier and F. Hapiot, Angew. Chem., Int. Ed., 2017, 56, 10564–10568.

[12] J. G. Hernández, Beilstein J. Org. Chem. , 2017, 13, 1463–1469.

[13] V. Štrukil and I. Sajko, Chem. Commun., 2017, 53, 9101-9104

[14] D. M. Baier, C. Spula, S. Fanenstich, S. Grätz and L. Borchardt, Angew. Chem. Int. Ed., 2023, 62, e202218719

[15] F. Luttringer, M. Lavayssiere, E. Rastoder, N. Salov, T. Gravelet, F. Quintin, J. Pinaud, F. Lamaty and X. Bantreil, RSC Mechanochem., 2025, 2, 108–115.

[16] M. Obst, R. S. Shaikh and B. König, React. Chem. Eng., 2017, 2, 472-478.

[17] F. Millward and E. Zysman-Colman, ACS Cent. Sci., 2026, 12, 17-27.

[18] F. Millward and E. Zysman-Colman, J. Am. Chem. Soc., 2025, 147, 22919-22931

[19] F. Millward and E. Zysman-Colman, Angew. Chem. Int. Ed., 2024, 63, e202316169.

[20] C. Spula, P. M. Preuß, L. Borchardt and S. Grätz, Chem. Eur. J., 2025, 31, e202501137.

[21] D. Kong, L. Yi, A. Nanni and M. Rueping, Nat. Commun., 2025, 16, 3983.

[22] A. Sobczyński, Ł. Duczmal and W. Zmudziński, J. Mol. Catal. A: Chem., 2004, 213, 225–230.

[23] T. Ohno, K. Sarukawa, K. Tokieda and M. Matsumura, J. Catal., 2001, 203, 82–86.

[24] T. Friščić, S. L. Childs, S. A. A. Rizvi and W. Jones, *CrystEngComm*, 2009, **11**, 418-426

[25] Y. Nosaka and A. Y. Nosaka, *Chem. Rev.*, 2017, **117**, 11302–11336

[26] B. Sheng, Y. Xie, Q. Zhao, H. Sheng and J. Zhao, Energy Environ. Sci., 2023, 16, 4612–4619.

[27] G. Chen, L. Chen, S.-M. Ng, W.-L. Man and T.-C. Lau, Angew. Chem. Int. Ed., 2013, 52, 1789–1791.

[28] A. Litke, Y. Su, I. Tranca, T. Weber, E. J. M. Hensen and J. P. Hofmann, J. Phys. Chem. C, 2017, 121, 7514–7524.

[29] M. A. Barakat, J. M. Tseng and C. P. Huang, Appl. Catal. B: Environ., 2005, 59, 99–104.

[30] X. Li, C. Chen and J. Zhao, Langmuir, 2001, 17, 4118–4122.

[31] R. G. Biswas, M. P. Croxall, R. T. Lawrence, R. Soong, M. C. Goh and A. J. Simpson, Nanoscale, 2022, 14, 9869

[32] M. P. Croxall, R. T. Lawrence, R. G. Biswas, R. Soong, A. J. Simpson and M. C. Goh, J. Phys. Chem. Lett., 2024, 15, 3653–3657

[33] J. T. Schneider, D. S. Firak, R. R. Ribeiro and P. Peralta-Zamora, Physical Chemistry Chemical Physics, 2020, 22, 15723–15733

[34] M.-A. Gatou, E. Fiorentis, N. Lagopati and E. A. Pavlatou, Water (Basel)., 2023, 15, 2773.

[35] C. Sol and R. J. D. Tilley, J. Mater. Chem., 2001, 11, 815–820.

[36] A. L. Patterson, Phys. Rev., 1939, 56, 978-982.

[37] H. C. Choi, Y. M. Jung and S. B. Kim, Vib. Spectrosc., 2005, 37, 33–38.

[38] V. Swamy, A. Kuznetsov, L. S. Dubrovinsky, R. A. Caruso, D. G. Shchukin and B. C. Muddle, Phys. Rev. B, 2005, 71, 184302.

[39] K. S. W. Sing, D. H. Everett, R. A. W. Haul, L. Moscou, R. A. Pierotti, J. Rouquérol and T. Siemieniewska, Pure Appl. Chem., 1985, 57, 603–619.

[40] J. Tauc, R. Grigorovici and A. Vancu, *Phys. Status Solidi B*, 1966, **15**, 627-637.

[41] H. Tang, F. Levy, H. Berger and P. E. Schmid, Phys. Rev B, 1995, 52, 11, 7771-7774

[42] B. Choudhury and A. Choudhury, Physica E, 2014, 56, 364–371.

[43] J. Augé, M.C. Scherrmann, New J. Chem. 2012, 36, 1091-1098

[44] N. Fantozzi, J.N. Volle, A. Porcheddu, D. Virieux, F. Garcia, E. Colacino, Chem Soc Rev, 2023, 52, 6680-6714

Data Availability Statement

View Article Online
DOI: 10.1039/D6MR00034G

Synergistic coupling of tribocatalysis and photocatalysis in a vibrating mill for the degradation of phenol over TiO_2

Guillaume Demily, Nicolas Kania, Anne Ponchel and Stéphane Menuel *

Univ. Artois, CNRS, Centrale Lille, Univ. Lille, UMR 8181, Unit´e de Catalyse et Chimie du Solide (UCCS), Rue Jean Souvraz, SP 18, 62300 Lens, France.

E-mail: stephane.menuel@univ-artois.fr

All data supporting this study are available within the article and it associated Electronic Supplementary Information (ESI) file. Any additional data related to this work are available from the corresponding author upon reasonable request.